Full Paper

Microcrystalline PETN Prepared Using Microfluidic Recrystallization Platform and Its Performance Characterization

Zhi Yang,[a, b, c] Peng Zhu,*[a, b, c] Qiu Zhang,[a, b, c] Jin-yu Shi,[a, b, c] Ke Wang,[a, b, c] and Rui-qi Shen[a, b, c]

Abstract: The particle size of explosives plays a key role in the short-duration pulse shock initiation, and explosives with small grain size and large specific surface area (SSA) generally have preferable sensitivity properties. We have constructed a high-throughput microfluidic recrystallization platform, aiming to prepare ultrafine pentaerythritol tetranitrate (PETN, $C(CH_2NO_3)_4$) via a precisely controllable solvent/nonsolvent recrystallization process. Through this platform, the recrystallized PETN was produced with a particle size of about 2 μm, and its SSA was above 70-fold that of the raw PETN. The X-ray diffraction results indicated that the raw and microcrystalline PETN had a similar diffraction spectrum. The thermal analysis demonstrated that com-pared with the raw PETN, the microcrystalline PETN revealed better decomposition performances. Importantly, the short-duration pulse shock initiation sensitivity of microcrystalline PETN pellets was evaluated when subjected to an exploding foil initiator. The shock initiation threshold results were as follows: 50% initiation voltage U (50%) = 1332 V, the corresponding capacitor storage energy was 195.2 mJ. Furthermore, the calculated shock pressure and shock duration imparting to the pellets were 9.61 GPa and 12.53 ns respectively, corresponding to the 3162 m/s threshold velocity. Finally, the enhanced sensitivity during the shock-to-detonation transition was further explained with the hot spot-based mechanism.

Keywords: Microfluidic platform · Ultrafine explosives · Shock initiation · Exploding foil initiator

1 Introduction

Explosives are high-energy-density energetic materials. Some meaningful progress has been achieved in the area of initiation performance. Nanoscale and microscale explosives are now attracting increasing attention, as they enable fast chemical energy release and great control over performance. The improvement of particle size to prepare ultrafine explosives with narrow size distribution and large specific surface area (SSA) is an important approach to improve initiation sensitivity [1–3]. Among the several synthesis methods of preparing ultrafine explosives, solvent/nonsolvent recrystallization is an old but promising approach [4,5].

Microfluidic technology allows the precise modulation of fluids such as explosive solutions down to nm and pL levels, so that the mixing efficiency and uniformity of fluids are significantly increased, compared with fluids prepared via the conventional batch reactor synthesis [6]. Moreover, synthesis with the microfluidic platform allows for a more continuous and safe operation, making it popular in the preparation of various narrow size-distributed ultrafine explosives [7].

Pentaerythritol tetranitrate (PETN, $C(CH_2NO_3)_4$) and hexanitrostilbene (HNS, $[C_6H_2(NO_2)_3CH]_2$) are two main explosive materials commonly utilized in exploding foil initiator (EFI), also called slapper detonator. This is due to their reliable threshold energy to short-duration pulse shock un-der high-speed impact with small-size thin flyer plates, causing a shock-to-detonation transition (SDT), and their excellent thermal and shock stabilities. The PETN structure is displayed in Figure 1. Numerous studies on HNS have been performed to meet the requirements of the output charge of EFI [8–10]. However, in previous studies, PETN only plays the role of an alternative explosive in EFI [11]. When impacted by the flyer, PETN performs with higher initiation sensitivity compared with HNS [12]. To the best of our knowledge, there are not many studies on the intrinsic improvements of PETN, aiming to improve the short-duration pulse shock initiation sensitivity. In this work, we pres-

[a] *Z. Yang, P. Zhu, Q. Zhang, J.-y. Shi, K. Wang, R.-q. Shen*
School of Chemical Engineering
Nanjing University of Science and Technology
Xiaolingwei Street 200, Xuanwu District, 210094, Nanjing, China
*e-mail: zhupeng@njust.edu.cn

[b] *Z. Yang, P. Zhu, Q. Zhang, J.-y. Shi, K. Wang, R.-q. Shen*
Key Laboratory of Special Energy Materials
Ministry of Education
Nanjing University of Science and Technology
Xiaolingwei Street 200, Xuanwu District, 210094, Nanjing, China

[c] *Z. Yang, P. Zhu, Q. Zhang, J.-y. Shi, K. Wang, R.-q. Shen*
Micro-Nano Energetic Devices Key Laboratory
Ministry of Industry and Information Technology
Nanjing University of Science and Technology
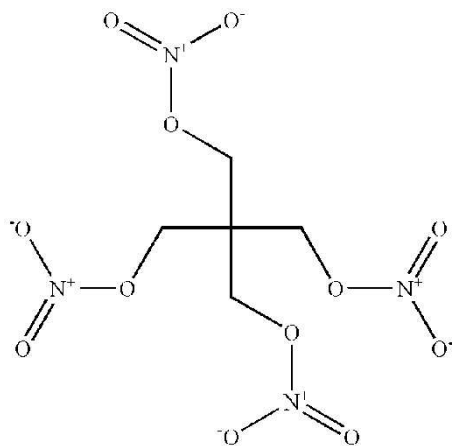*Xiaolingwei Street 200, Xuanwu District, 210094, Nanjing, China*

Figure 1. PETN structure.

ent a homemade microfluidic platform to prepare ultrafine PETN via the solvent/nonsolvent recrystallization process, and the results indicate that the raw PETN was greatly optimized. Comparative studies on the microcrystalline PETN and raw PETN were further performed, considering several properties, including the short-duration pulse shock initiation sensitivity, which was determined using an EFI.

2 Experimental Section

2.1 Materials

In this work, the crude PETN explosive was supplied by a factory, then recrystallized from the conventional batch reactor in our laboratory. The solvent utilized for dissolving PETN was AR-grade dimethyl sulfoxide (DMSO), purchased from Aladdin Co., Ltd. The raw PETN was saturated in DMSO, then generated after the vaporization of DMSO. The nonsolvent used in the microfluidic recrystallization platform was homemade ultrapure water.

2.2 Preparation of Microcrystalline PETN

Figure 2a shows the overall microfluidic recrystallization platform, including the N_2 pressure source, injection pump, solvent (DMSO), nonsolvent (ultrapure water), oscillator, micro-mixer, and container. The oscillator plays a key role in the platform, which is made up of two chambers and an intermediate metal diaphragm. Under the impelling pressure from the nonsolvent, the diaphragm oscillates between the first and second chambers within its elastic deformation boundary, eventually forming an oscillatory flow. Therefore, the accumulation of crystalline grains can be avoided under the high turbulence from the oscillatory flow, and continuous flow along the microchannels is ensured.

Another key component in the platform is the double-chamber micro-mixer (Figure 2b), which was assembled by bonding a silicon chip with a glass chip, making it resistant to the solution corrosion and easy to monitor. Specifically, the effective structures were first carved on the silicon chip surface within 0.5 mm and then combined with the glass chip. The micro-mixer consisted of two inlet channels, an outlet channel, and a double chamber for fully mixing solvent and nonsolvent. The two chambers had the same size of 5.0 mm diameter and 0.5 mm depth, and the widths of the inlet and outlet channels were 0.5 mm. The solvent and nonsolvent separately flow into the double-chamber micro-mixer, then reach a high mixing degree in the chamber. The two above-mentioned components in the platform contribute to the batch preparation of ultrafine substances such as microcrystalline PETN with uniform particles.

The supersaturation of solution determines the rapid nucleation and the following product with small-size crystals and narrow particle-size distribution (PSD) during the solvent/nonsolvent recrystallization process. Therefore, we first tested the PETN solubility in DMSO, and the PETN-to-DMSO ratio was determined as about 100 mg: 1 mL. Ultrapure water was selected as the nonsolvent since it is easily accessible, and PETN is insoluble in it. Furthermore, DMSO and ultrapure water are completely miscible to meet the prerequisite requirement of solvent/nonsolvent recrystallization. In the experiment process, ultrapure water stored in a high-pressure liquid tank flowed into the microchannel at a fixed rate of 20 mL/min under N_2 pressure source. The metal diaphragm was caused to oscillate after the water flow. The solution of 500 mg PETN in 5 mL DMSO was drawn into a 10 mL graduated syringe, and then regulated by a high-precision injection pump with a controllable flow rate.

We conducted experimental research from 0.1 mL/min to 1.0 mL/min of the nonsolvent, because it was considered that the different flow rate and the operation feasibility. The influence of the flow ratio of nonsolvent to solvent on the explosive morphology was studied. The solvent and nonsolvent were fully mixed in the double-chamber micro-mixer, and the product was collected at the outlet by a container. The yield of microcrystalline PETN reached about 85% after filtration and drying processes. This microfluidic recrystallization platform had been designed into parallel structures to construct a lab-on-table, with a production rate of up to 1 g/h or even higher.

2.3 Performance Characterization

The crystal morphology was obtained via field-emission scanning electron microscopy (FE-SEM, Quanta 400 FEG). The PSD was measured with a particle size analyzer (MS3000, Malvern). The composition and crystallization were characterized via X-ray diffraction (XRD, Rigaku Smartlab9). Differential scanning calorimetry (DSC) and thermog-
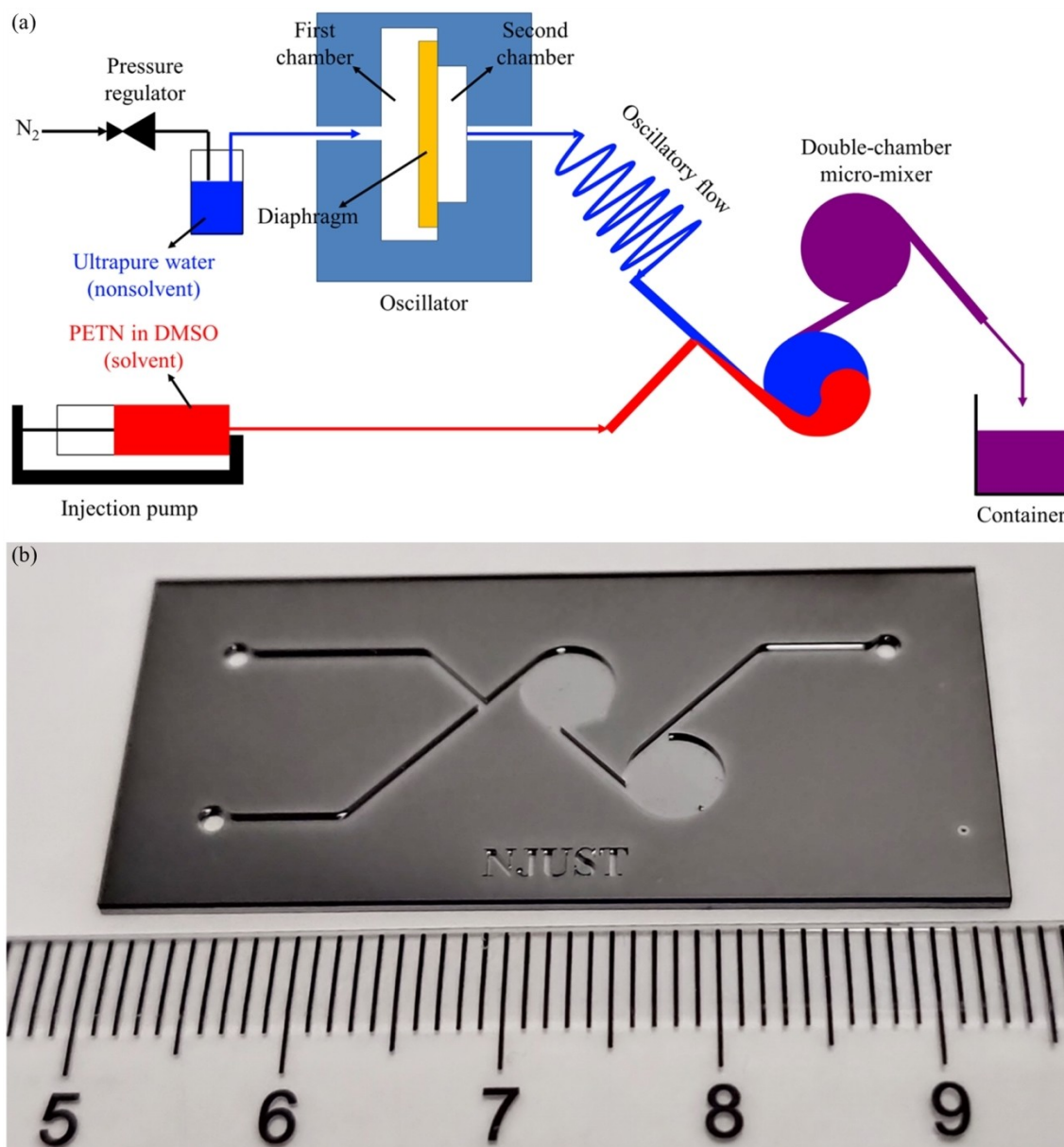
Figure 2. Microfluidic recrystallization platform for microcrystalline PETN (a) and double-chamber micro-mixer (b).

ravimetric analysis (TGA) were performed on STA 449C, with heating rates of 5 °C/min, 10 °C/min, 15 °C/min, and 20 °C/min in Ar atmosphere. The sample mass of explosives was about 5 mg. 20 PETN pellets were die-pressed in a mould with the pressure of 250 MPa. The prepared pellets had the size of 2.3 mm (Φ) × 2.0 mm (h) with about 1.65 g/cm³ density. PETN pellets were subjected to EFI after the basic performance analysis was completed, to directly check their short-duration pulse shock initiation sensitivity.

3 Results and Discussion

3.1 Crystal Morphology

We utilized FE-SEM to photograph the PETN crystals with fitting magnifications (Figure 3). The single crystal of raw PETN was tetragonal, and a spherical cluster consisted of a group of crystals with an overall size of about 300 μm. Via the microfluidic recrystallization platform, the particle size of the obtained PETN was largely reduced to about 2 μm, which was at the microcrystalline level.

Furthermore, as displayed in Figures 3b–d, the microcrystalline PETN with a solvent flow rate of 0.1 mL/min had
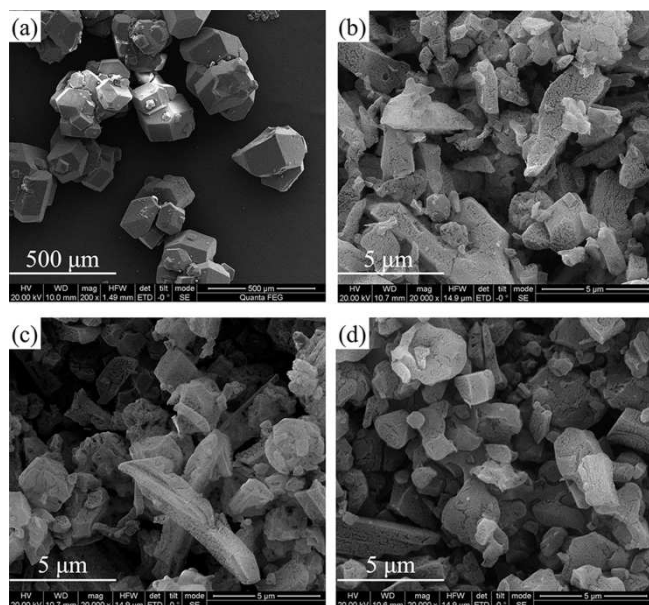
Figure 3. SEM images of raw PETN (a) and microcrystalline PETN with solvent flow rates of 1.0 mL/min (b), 0.5 mL/min (c), and 0.1 mL/min (d).

Figure 4. Particle-size distributions of raw PETN (a) and microcrystalline PETN (b).

a smaller size and more uniform morphology than those with 0.5 mL/min and 1.0 mL/min. This may be because at the lower solvent flow rate less PETN is available for crystal growth after particles nucleated, and the aggregation of numerous precipitated particles can be avoided. Therefore, for further studies, only microcrystalline PETN with 0.1 ml/min was adopted.

3.2 Particle-Size Distribution

The PSD was tested using the MS3000 particle size analyzer by dispersing PETN bulk into ultrapure water. This analysis result was based on the Mie scattering model, with the refractive index of PETN grain as 1.553 [13]. Three key parameters to characterize the PSD are D (10), D (50), and D (90), whose definitions are the particle sizes corresponding to cumulative particle distribution of 10%, 50%, and 90% respectively. D (50) is also called median particle size, which means the particle volume fractions above or below this particle size are all 50%. Figure 4a shows the PSD plot of raw PETN, and D (10) = 242 µm, D (50) = 363 µm, and D (90) = 536 µm. The corresponding distribution results of microcrystalline PETN are 2.42 µm, 6.45 µm, and 17.3 µm (Figure 4b). The particle size was defined by the diameter of an equivalent sphere. Figure 3 shows that the crystalline shape of the raw PETN was sphere-like, so the results practically described its real PSD. However, the equivalent diameter of the microcrystalline PETN with an irregular crystal appearance was somewhat enlarged. Although this test method amplified the result, the D (50) of the microcrystalline PETN
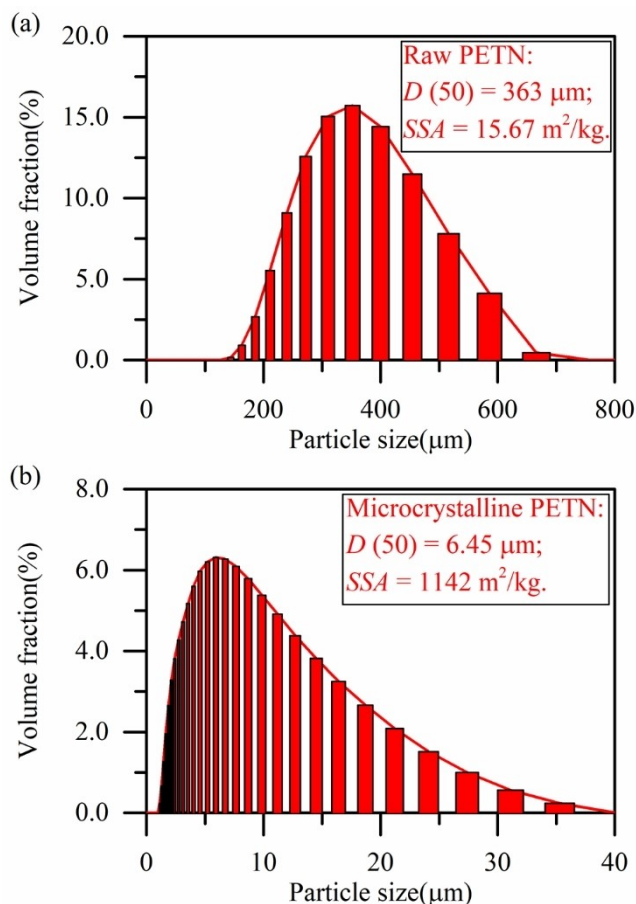
was near 1/60 of that of the raw PETN. Besides, the SSA of the microcrystalline PETN was 1142 m²/kg, which was above 70-fold that of the raw PETN. The microcrystalline PETN with narrow PSD had a large SSA, which is beneficial to improve its initiation sensitivity under short-duration pulse shock.

3.3 Composition and Crystalline State

Figure 5 illustrates the PETN diffraction peak intensity as a function of the diffraction angle (2θ). The diffraction spectrum of the microcrystalline PETN was similar to that of the raw PETN, indicating that the two had identical crystal structures. Furthermore, there was no characteristic peak from any impurities, which implies that the microcrystalline PETN had high purity.

3.4 Thermal Decomposition Behavior

The response of explosives to thermal stimulus directly affects their stability and sensitivity, so it is essential to test the relationship of thermophysical properties with temperature. In this work, thermal decomposition properties were experimentally investigated on a DSC-TGA instrument (STA 449C) in the Ar atmosphere.

Figure 6a displays the DSC curves with a heating rate (β) of 10 °C/min. Both the raw PETN and microcrystalline PETN first absorbed heat in the melting period and then decomposed with a large amount of heat output (ΔH). The endothermic peak and exothermic peak of the raw PETN were 143.3 °C and 208.4 °C, respectively, which agree with the findings of the previous study [14]. The two peaks of the microcrystalline PETN were about 2 °C earlier than those of the raw PETN, after taking the measurement error of 0.1 °C into consideration. This phenomenon may be due to the sensitization from small particle size and large SSA [15]. The results also show that as the heating rate increased from 5 °C/min to 20 °C/min, the decomposition temperature of the raw and microcrystalline compounds increased. Furthermore, Figure 6b displays the TGA profiles. The two TGA trends of the raw PETN and microcrystalline PETN were basically the same, with mass-loss rates of 95.12% and 95.37%, respectively. The onset temperature of mass loss of the raw PETN was 151.2 °C, but that for the microcrystalline PETN was 148.5 °C, because of the earlier melting reaction. Similar phenomena were observed at other tests with heating rates of 10 °C/min, 15 °C/min, and 20 °C/min.

The activation energy (E_a), also called threshold energy, represents the minimum energy required for a chemical reaction to occur, which indicates how easy the reaction is. In combination with the T_{peak} values achieved at 10 °C/min, 15 °C/min, and 20 °C/min, two Kissinger's plots with $\ln(\beta/T_{peak}^2)$ as a function of $1/T_{peak}$ were obtained (Figure 7) [16]. The E_a of the microcrystalline PETN was 108.8 kJ/mol,
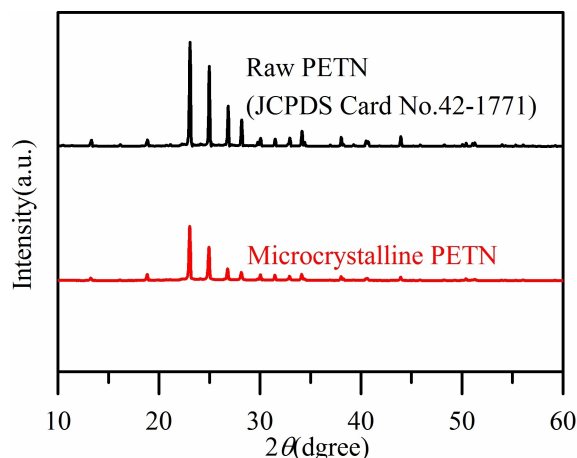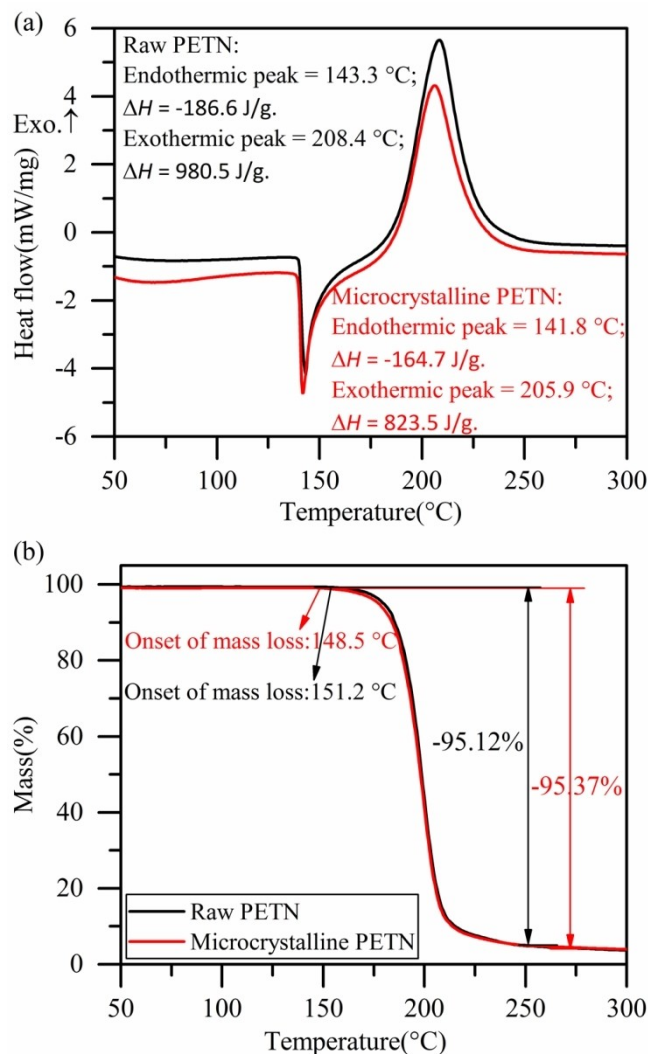
Figure 6. DSC profiles (a) and TGA curves (b) of raw and microcrystalline PETN with a heating rate of 10 °C/min.

as determined based on the slope of Kissinger's plot and the gas constant ($R = 8.134$ J/mol/K); this value was 15% lower than that of the raw PETN (128.6 kJ/mol). The E_a of microcrystalline PETN was rather low compared to the literature value [17]. We hold that it is also the sensitization resulted from the small particle size and large SSA, which is conducive to the chemical reaction.

3.5 Shock Initiation Validation by EFI

3.5.1 EFI-Based Fireset for PETN Pellets

We introduced an EFI-based fireset to directly estimate the short-duration pulse shock initiation sensitivity of PETN pellets. The schematic diagram and photograph of the fireset are displayed in Figure 8. This fireset was a series circuit, in-
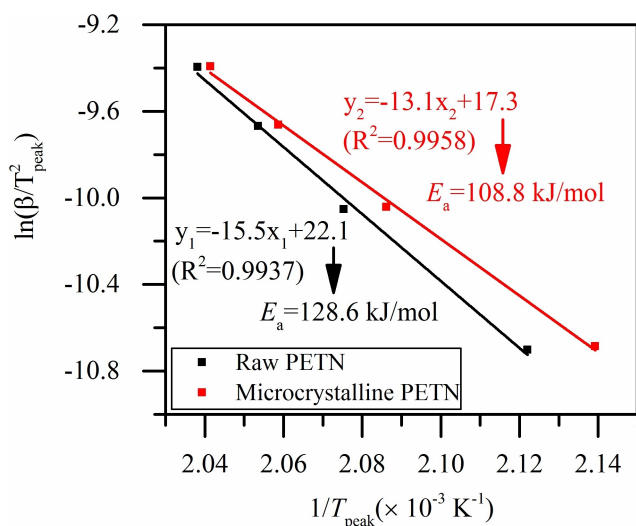
Figure 5. XRD spectra of raw and microcrystalline PETN.

Figure 7. Kissinger's plots of raw PETN and microcrystalline PETN.

Table 1. Structural parameters of EFI.

Structures	Parameters
Ceramic substrate	4.2 mm (*l*) ×3.0 mm (*w*) ×0.6 mm (*h*)
Cu bridge foil	400 μm (*l*) ×400 μm (*w*) ×3.6 μm (*h*)
PC flyer	600 μm (*Φ*) ×25 μm (*h*)
SU-8 barrel	600 μm (*Φ*) ×400 μm (*h*)
PETN pellet	2.3 mm (*Φ*) ×2.0 mm (*h*); about 1.65 g/cm³.

through a DC power supply before the switch is closed; (2) the large pulse current from the capacitor flows into Cu bridge foil after the switch is closed. As a result, an electrical explosion occurs with violent phase transformation; (3) High-temperature and high-pressure plasma and gases (also including the frontal shock waves) from the electrical explosion shear the PC flyer layer and then drive the flyer in the SU-8 barrel; (4) the PC flyer reaches several km/s when out of the barrel, and the PETN pellet is detonated when the shock wave pressure and duration exceed the initiation threshold.

3.5.2 Determination of Threshold Voltage with Langlie Method

Langlie method, a statistical method with various steps, was adopted to check the initiation threshold of microcrystalline PETN. In our test, the discharge voltage from the high-voltage capacitor was selected as the variable stimulus. According to our experience, the low voltage limit was set as 600 V, and the upper limited voltage was 1800 V. Fur-

cluding a high-voltage capacitor ($C = 0.22$ μF), a pulse power switch, and an EFI. The lumped inductance and resistance of the fireset were about 40 nH and 140 mΩ, respectively. The EFI was a core component in this detonation output device, and it was composed of a ceramic substrate, Cu bridge foil, Parylene C (PC) flyer layer, SU-8 barrel, and PETN pellet. The PETN pellets were pressed to 90%–95% theoretical maximum density (TMD, 1.773 g/cm³). The EFI structural parameters are listed in Table 1 [18,19].

The working process of the EFI-based fireset is briefly described as follows: (1) a high-voltage capacitor is charged
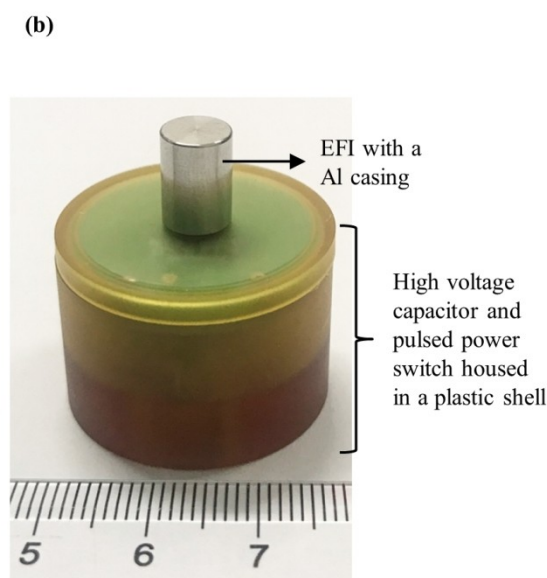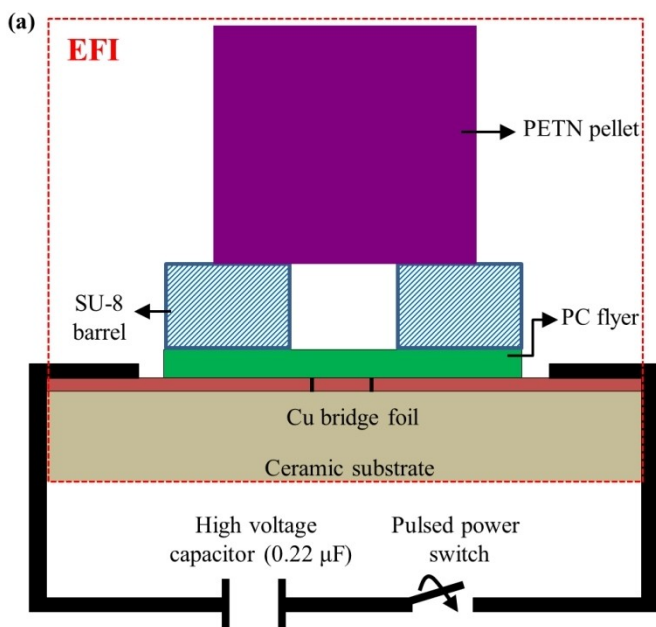

Figure 8. Schematic diagram (a) and photograph (b) of the EFI-based fireset.

thermore, 20 attempts were chosen as the experimental termination criterion, and the successful responses were defined as the detonation of PETN pellets. The results showed that the detonation responses were 9 shots in the range of 600 V to 1800 V.

The sensitivity threshold was calculated according to the maximum likelihood estimation algorithm by assuming it obeys the normal distribution. The results indicated the following: 50% threshold voltage U (50%) = 1332 V and 99.9% threshold voltage U (99.9%) = 1414 V. We further obtained the matched capacitor storage energy as E_C (50%) = 195.2 mJ and E_C (99.9%) = 220.0 mJ. It should be noted that the raw PETN pellets still failed to be initiated when the discharge voltage was increased to 3000 V (corresponding capacitor storage energy was 990.0 mJ), and it was meaningless to further increase the voltage. Due to the grain size (about 300 μm) was almost identical to the flyer diameter (600 μm), we are convinced that the particles to be impacted by the flyer were rather few, and then raw PETN pellets cannot be detonated by the small-size thin flyer disk.

3.5.3 Real-Time Flyer Velocity

The flyer velocity is a key parameter affecting the shock initiation of explosives. Compared with the theoretical calculation of flyer velocity that is dependent on energy conversion coefficients, the measured instruments offer a real velocity. Photonic Doppler velocimetry (PDV) is an effective vehicle used for recording interference signals to reconstruct the acceleration progress of small-size targets based on the laser Doppler effect [20], which is used to test the real-time flyer velocity.

Figure 9 displays the real-time velocity of the PC flyer at 1300 V, 1400 V, and 1500 V, as well as the acceleration distance at 1400 V, determined via PDV. The flyer velocity
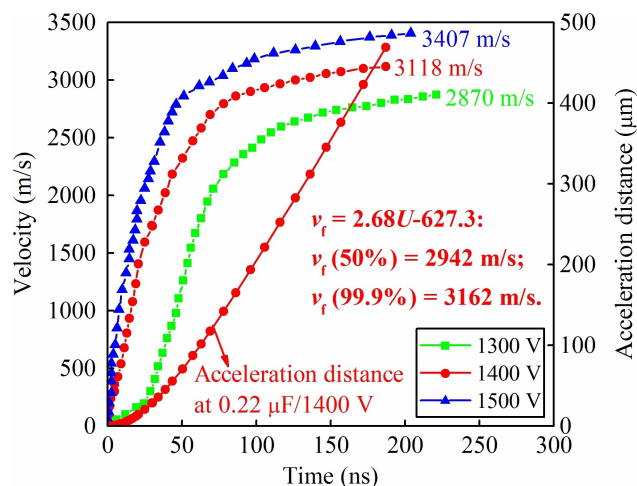

Figure 9. Real-time flyer velocities under different voltages and acceleration distance at 1400 V (0.22 μF).

curve was divided into two stages: the rapid growth stage driven by shock waves from the electrical explosion; and the slow growth stage originated from the expansion effect of plasma and gases. The PC flyer at the peak moment was accelerated with a distance of 469 μm under 0.22 μF/1400 V, which indicated that the flyer was located beyond the barrel with 69 μm. This real acceleration distance from the PDV test also illustrates the relatively rational design of the SU-8 barrel height. Furthermore, the relationship between the peak velocity and the discharge voltage was approximately linear within 1300 V to 1500 V. Therefore, the peak velocities corresponding to U (50%) and U (99.9%) were calculated as v_f (50%) = 2942 m/s and v_f (99.9%) = 3162 m/s, respectively.

We calculated the threshold kinetic energy based on the threshold velocity. The kinetic energy of PC flyer imparting to PETN pellets is expressed as

$$E_k = \frac{1}{2}mv_f^2, \tag{1}$$

where E_k is the kinetic energy of the PC flyer, m is the flyer mass, and v_f is the flyer velocity.

Therefore, we obtained the threshold kinetic energies combining with the structural parameters of the PC flyer and the threshold velocities: E_k (50%) = 39.46 mJ and E_k (99.9%) = 45.58 mJ. It can be further concluded that the kinetic energy was about 20% of the capacitor storage energy.

3.5.4 Determination of Shock Pressure and Duration [21–23]

There is an important identical equation in the moment of the flyer impact on the explosive based on the momentum theorem:

$$p_e A_f t = A_f D_e t \rho_e u_e, \tag{2}$$

where p_e is the shock pressure of flyer imparting to explosives, A_f is the flyer area, t is the interaction time, D_e is the shock wave velocity in the explosives, ρ_e is the density of PETN pellet, and u_e is the particle velocity of PETN.

Equation (2) is simplified as

$$p_e = \rho_e D_e u_e. \tag{3}$$

According to Newton's third law of motion, the PC flyer will be subject to the reaction force from the PETN pellet:

$$p_f = \rho_f D_f(v_f - u_f), \tag{4}$$

where p_f is the shock pressure of the PETN pellet on the PC flyer, D_f is the shock wave velocity in the PC flyer, ρ_f is the density of the PC flyer, and u_f is the particle velocity of PC flyer.

A linear relationship exists between the shock wave velocity and the particle velocity:

$$D_f = c_f + a(v_f - u_f), \tag{5}$$

where c_f and a are Hugoniot coefficients of the PC flyer, specifically c_f is the acoustic speed in the PC flyer, and a is a linear coefficient.

The shock pressure can be derived using Equations (4) and (5):

$$p_f = \rho_f[c_f + a(v_f - u_f)](v_f - u_f). \tag{6}$$

Both the particle velocity and shock pressure at the interface are continuous, so

$$u = u_f = u_e, \ p = p_f = p_e \tag{7}$$

Therefore, the particle velocity and the shock pressure can be obtained using Equations (3), (6), and (7).

A shock wave emerges in the PC flyer since the shock impedance (ρD) of the PETN pellet is larger than that of the flyer. Subsequently, a rarefaction wave is reflected when the shock wave arrives at the free surface of the flyer. The shock duration is the time before the rarefaction wave catches up the shock wave, so the shock duration is calculated with the PC flyer thickness, expressed as (8):

$$\tau = \frac{2d_f}{D_f}, \tag{8}$$

where d_f is the thickness of the PC flyer.

The Hugoniot data of Kapton were adopted to calculate the shock pressure and duration, due to the similar property between PC and Polyimide (PI or Kapton). Coefficients for the calculation are listed in Table 2.

The calculated 99.9% shock pressure (p (99.9%)) and shock duration (τ (99.9%)) were 9.61 GPa and 12.53 ns respectively, according to the measured velocity of 3162 m/s. It is indicated that this EFI-based fireset is feasible to initiate the PETN pellets due to such high shock pressure and duration [12,24]. In the future, an initiation criterion can be fitted with several shock pressures and durations based on the several flyer thicknesses, so we can assess the initiation results under different flyer thicknesses and discharge voltages. Since the raw PETN pellets cannot be detonated by the small-size thin PC flyer, the relevant threshold data are not available. In summary, the characteristic properties of the microcrystalline and raw PETN are listed in Table 3.

3.6 Hot Spot-Based Explanation for SDT

The microcrystalline PETN is one of the heterogeneous explosives because there are imperfections or defects (such as pores and cracks) at the mesoscale. The hot spot mecha-

Table 2. Coefficients for the shock pressure and shock duration.

Materials	ρ (g/cm³)	c (m/s)	a	D (m/s)
PETN	1.65	/	/	~4500 [12]
PC	1.29	930 [24]	1.64 [24]	/

Table 3. Comparison of characteristic properties of raw PETN and microcrystalline PETN.

Properties	Raw PETN	Microcrystalline PETN
Particle size (μm)	~300	~2
SSA (m²/kg)	15.67	1142
Endothermic peak (°C)	143.3	141.8
Exothermic peak (°C)	208.4	205.9
ΔH with10°C /min (J/g)	980.5	823.5
E_a (kJ/mol)	128.6	108.8
Thermogravimetric loss	95.12%	95.37
U (50%) (V)	/	1332
E_c (50%) (mJ)	/	195.2
v_f (50%) (m/s)	/	2942
E_k (50%) (mJ)	/	39.46
p (99.9%) (GPa)	/	9.61
τ (99.9%) (ns)	/	12.53

nism has generally been proposed to be responsible for the SDT in heterogeneous explosives [25–28]. The process of flyer impacting the explosive proceeds quickly, which can be regarded as an adiabatic compression process because the heat exchange between the explosive and surrounding environment occurs late. First, hot spots are formed in some local regions (hot spot formation stage) after the short-duration pulse shock enters the PETN pellet, due to the voids collapse from the impact of the incident shock wave on the defects. The decomposition reaction with chemical energy release, burning or combustion, and low-velocity detonation successively spread around the hot spot (hot spot growth stage). Finally, steady detonation occurs.

The temperature of the gas after adiabatic compression can be solved using [29]

$$\frac{T_2}{T_1} = \left(\frac{p_2}{p_1}\right)^{\frac{\gamma-1}{\gamma}} = \left(\frac{V_1}{V_2}\right)^{\gamma-1}, \tag{9}$$

where T_1, p_1, and V_1 are the temperature, pressure, and volume of the initial state, respectively; T_2, p_2, and V_2 are the temperature, pressure, and volume of the terminal status, respectively; and γ is the specific heat ratio or adiabatic index.

From the hotspot-based explanation, we know that the initiation sensitivity of PETN is determined by the temperature and hot spot number. The microcrystalline PETN has a smaller particle size and a larger SSA than the raw PETN so that the pores between the grains also have a smaller volume and a larger SSA. High porosity provides more collapse sites to generate high temperatures for the hot spots formation. Therefore, more heat is emitted from the hot spots,

which is beneficial to improve the short-duration pulse shock initiation sensitivity and reduce the initiation threshold. This hot spot-based explanation for the improved sensitivity is also verified by the preceding thermal decomposition test, which shows a lower decomposition temperature for microcrystalline PETN, and contributes to the hot spot formation and the following energy release. Furthermore, the defects between the particles are so few that they can be ignored when the particle size is sufficiently small, and the explosive should be regarded as a homogeneous explosive. At this time, not many hot spots are generated after the flyer impact effect, so the sensitivity may no longer obey the law of heterogeneous explosives.

4 Conclusion

Raw PETN was recrystallized with the solvent/nonsolvent process via a homemade microfluidic platform. The obtained microcrystalline PETN had a small particle size of about 2 μm, and its SSA was above 70-fold that of the raw PETN. Thermal analysis showed that the microcrystalline PETN had better decomposition property owing to the sensitization from its smaller grain size and larger SSA. Importantly, the short-duration pulse shock initiation sensitivity of the microcrystalline PETN pellets was gauged by an EFI. The results indicated the following: 50% threshold voltage U (50%) = 1332 V, the corresponding E_C (50%) = 195.2 mJ, and v_f (50%) = 2942 m/s. The shock pressure and duration for the pellets were calculated using the measured velocity from PDV. We further explain the improved initiation sensitivity in the SDT with the hot spot-based mechanism. The microfluidic recrystallization platform has the properties of inherent safety and high throughput, so it can be applied for the batch preparation of other ultrafine explosives with desired sensitivities.

Acknowledgements

Data Availability Statement

No Data available.

References

[1] R. E. Setchell, Grain-size effects on the shock sensitivity of hexanitrostilbene (HNS) explosive, *Combust. Flame* **1984**, *56*, 343–345. doi:10.1016/0010-2180(84)90068-3.

[2] C. An, S. Xu, Y. R. Zhang, B. Ye, X. Geng, J. Y. Wang, Nano-HNS particles: mechanochemical preparation and properties investigation, *J. Nanomater.* **2018**, *2018*, 1–7. doi:10.1155/2018/9436089.

[3] J. Wang, W. Cao, X. Guo, B. Cheng, L. Zhao, R. Liu, X. Chen, Effect of microstructure on short pulse duration shock initiation of TATB and initial response mechanism, *Def. Technol.* **2020**, *16*, 374–380.

[4] J. Wang, H. Huang, W. Xu, Y. Zhang, B. Lu, R. Xie, P. Wang, N. Yun, Prefilming twin-fluid nozzle assisted precipitation method for preparing nanocrystalline HNS and its characterization, *J. Hazard. Mater.* **2009**, *162*, 842–847. doi:10.1016/j.jhazmat.2008.05.107.

[5] J. Kaur, V. P. Arya, G. Kaur, T. Raychaudhuri, P. Lata, Evaluation of ultrasonic treatment for the size reduction of HNS and HMX in comparison to solvent-antisolvent crystallization, *Propellants Explos. Pyrotech.* **2012**, *37*, 662–669. doi:10.1002/prep.201100072.

[6] Y. Liu, X. Jiang, Why microfluidics? merits and trends in chemical synthesis, *Lab Chip* **2017**, *17*, 3960–3978. doi:10.1039/c7lc00627f.

[7] M. Movsisyan, E. I. P. Delbeke, J. K. E. T. Berton, C. Battilocchio, S. V. Ley, C. V. Stevens, Taming hazardous chemistry by continuous flow technology, *Chem. Soc. Rev.* **2016**, *45*, 4892–4928. doi:10.1039/c5cs00902b.

[8] B. T. Neyer, L. Cox, T. Stoutenborough, R. Tomasoski, HNS-IV explosive properties and characterization tests, *39th AIAA/ASME/SAE/ASEE Joint Propulsion Conference and Exhibit*, Huntsville, AL, USA, July 20–24, **2003**, p. 5138. doi:10.2514/6.2003–5138.

[9] E. Hasman, M. Gvishi, A. Solomonovici, The initiation threshold sensitivity of HNS explosive as a function of its grain size, *Propellants Explos. Pyrotech.* **1987**, *12*, 130–132. doi:10.1002/prep.19870120405.

[10] J. Waschl, D. Richardson, Effect of specific surface area on the sensitivity of hexanitrostilbene to flyer plate impact, *J. Energ. Mater.* **1991**, *9*, 269–282. doi:10.1080/07370659108018628.

[11] W. L. Shaw, C. Grant, C. Fox, H. E. Reinstein, T. M. Willey, M. Bagge-Hansen, M. H. Nielsen, J. A. Hammons, L. M. Lauderbach, R. L. Hodgin, R. H. Gee, Evaluating the ignitibility of PETN by aged exploding foil initiators, *International Detonation Symposium*, Cambridge, MD, USA, July 15–20, **2018**.

[12] A. C. Schwarz, *New technique for determining the shock initiation sensitivity of explosives*, Report SAND-77-0416 C, Sandia Laboratory, Albuquerque, NM, USA, **1977**.

[13] K. Wakabayashi, T. Matsumura, Y. Nakayama, M. Koshi, Refractive index of pentaerythritol tetranitrate single crystals at 532 nm, *Sci. Technol. Energ. Mater.* **2013**, *74*, 80–83.

[14] J. Lee, C. Hsu, C. Chang, A study on the thermal decomposition behaviors of PETN, RDX, HNS and HMX, *Thermochim. Acta* **2002**, *392–393*, 173–176. doi:10.1016/S0040-6031(02)00099-0.

[15] M. R. Sovizi, S. S. Hajimirsadeghi, B. Naderizadeh, Effect of particle size on thermal decomposition of nitrocellulose, *J. Hazard. Mater.* **2009**, *168*, 1134–1139. doi:10.1016/j.jhazmat.2009.02.146.

[16] H. E. Kissinger, Reaction kinetics in differential thermal analysis, *Anal. Chem.* **1957**, *29*, 1702–1706. doi:10.1021/ac60131a045.

[17] R. V. Tsyshevsky, O. Sharia, M. M. Kuklja, Molecular theory of detonation initiation: insight from first principles modeling of the decomposition mechanisms of organic nitro energetic materials, *Molecules* **2016**, *21*, 236. doi:10.3390/molecules21020236.

[18] C. Xu, P. Zhu, K. Chen, W. Zhang, R. Shen, Y. Ye, A highly integrated conjoined single shot switch and exploding foil initiator chip based on MEMS technology, *IEEE Electron Device Lett.* **2017**, *38*, 1610–1613. doi:10.1109/LED.2017.2752749.

[19] Z. Yang, G. Q. Zheng, P. Zhu, C. Xu, Q. Zhang, K. Wang, R. Shen, Design, fabrication and characterization of an electrical-explosively actuated MEMS flyer-accelerator inserted with parallel bridge foils, *Eur. Phys. J. Appl. Phys.* **2020**, *91*, 10301. doi:10.1051/epjap/2020200042.

[20] D. H. Dolan, Extreme measurements with photonic doppler velocimetry (PDV), *Rev. Sci. Instrum.* **2020**, *91*, 051501. doi:10.1063/5.0004363.

[21] F. E. Walker, R. J. Wasley, Critical energy for shock initiation of heterogeneous explosives, *Explosivstoffe* **1969**, *17*, 9–13.

[22] H. R. James, An extension to the critical energy criterion used to predict shock initiation thresholds, *Propellants Explos. Pyrotech.* **1996**, *21*, 8–13. doi:10.1002/prep.19960210103.

[23] Q. Chen, Y. Li, T. Ma, Characterization of the super-short shock pulse generated by an exploding foil initiator, *Sens. Actuators A Phys.* **2019**, *286*, 91–97. doi:10.1016/j.sna.2018.12.018.

[24] M. D. Bowden, M. P. Maisey, Determination of critical energy criteria for hexanitrostilbene using laser-driven flyer plates, *Proceedings of SPIE*, San Diego, CA, USA, September 3, **2008**. doi:10.1117/12.796271.

[25] C. A. Handley, B. D. Lambourn, N. J. Whitworth, H. R. James, W. J. Belfield, Understanding the shock and detonation response of high explosives at the continuum and meso scales, *Appl. Phys. Rev.* **2018**, *5*, 011303. doi:10.1063/1.5005997.

[26] J. Zhang, T. L. Jackson, Effect of microstructure on the detonation initiation in energetic materials, *Shock Waves* **2017**, *29*, 327–338. doi:10.1007/s00193-017-0796-7.

[27] C. D. Yarrington, R. R. Wixom, D. L. Damm, Shock interactions with heterogeneous energetic materials, *J. Appl. Phys.* **2018**, *123*, 105901. doi: 10.1063/1.5022042.

[28] T. Zhou, J. Lou, Y. Zhang, H. Song, F. Huang, Hot spot formation and chemical reaction initiation in shocked HMX crystals with nanovoids: a large-scale reactive molecular dynamics study, *Phys. Chem. Chem. Phys.* **2016**, *18*, 17627–17645. doi:10.1039/c6cp02015a.

[29] W. P. Bassett, B. P. Johnson, N. K. Neelakantan, K. S. Suslick, D. D. Dlott, Shock initiation of explosives: high-temperature hot spots explained, *Appl. Phys. Lett.* **2017**, *111*, 061902. doi:10.1063/1.4985593.